Supporting Information

Lang et al. 10.1073/pnas.1503328112

SI Text

Stochastic Behavior of Fibril Formation Kinetics. The aggregation kinetics of all variants of SOD1 studied here are quite variable but can be fitted to a generalized γ-distribution (Fig. 1*D*, *Inset*) (7):

$$g(x;\ \alpha,\beta) = \xi\beta^{\alpha}\frac{1}{\Gamma(\alpha)}x^{\alpha-1}e^{-\beta x}, \qquad \text{[S1]}$$

where α and β are shape and rate parameters, respectively, and ξ is a normalization factor. In this distribution, the expected mean is $\alpha\beta^{-1}$, and the SD is $(\alpha\beta^{-2})^{1/2}$, which means that the SD is expected to scale linearly with the mean value. The linear correlation between the measured $\tau_{1/2}$ and the experimental SD is shown in Fig. S1 and is in good agreement with earlier findings for urea unfolded SOD1 (7).

Correction for Varying Intrinsic Aggregation Propensity. It is safe to assume that the observed aggregation kinetics are a function of effective concentration of aggregation prone material as well as the intrinsic aggregation propensity of that material. In the case of a natively folded protein (N), the effective concentration is, in fact, the concentration of unfolded material, [D], which is directly reflected in the equilibrium constant $K_{DN} = [N]/[D]$, which gives the effective concentration

$$[D] = c^{\text{total}}\frac{K_{DN}}{1+K_{DN}}, \qquad \text{[S2]}$$

where c^{total} is the total protein concentration. The intrinsic aggregation propensity (for example, caused by modifications affecting hydrophobicity and/or electrostatics) can be transferred into a general expression for aggregation kinetics, which can be written

$$\frac{M(t)}{c^{\text{tot}}} = G\big(F([D],k_i),\ H([D],k_j)\big), \qquad \text{[S3]}$$

where $F([D],k_i)$ is a general function describing the aggregate growth, and $H([D],k_j)$ is a corresponding general function describing primary nucleation. In case of a system where the aggregation kinetics are dominated by secondary pathways rather than primary nucleation, the observable $\tau_{1/2}$ (i.e., the time for one-half completion for aggregation of the monomer pool) and ν_{max} (the maximum growth rate) can be described as a function of the effective concentration, reaction orders, and a number of microscopic kinetic rates, k_i. In addition, for those systems, it has been shown that $\tau_{1/2}$ and ν_{max} are strongly correlated (4), and Eq. **S3** can, thus, be written as

$$\tau_{1/2} \propto \nu_{max} \propto F([D],k_i). \qquad \text{[S4]}$$

The relative change in the intrinsic aggregation propensity (p) for a modified protein relative to a reference can be measured as the change in the observable $\tau_{1/2}$ relative to the unbiased reference molecule at conditions where [D] is constant. This relation gives a correction factor for the function F:

$$\tau_{1/2}^{\text{corr}} = \frac{\tau_{1/2}^{\text{mutant,5 M urea}}}{\tau_{1/2}^{\text{REF, 5 M urea}}}\tau_{1/2}^{\text{obs,0 M urea}} = \frac{p^{\text{mutant}}}{p^{\text{pwt}}}\tau_{1/2}^{\text{obs,0 M urea}} = \frac{p^{\text{mutant}}}{p^{\text{pwt}}}F([D],k_i). \qquad \text{[S5]}$$

Here, we determined the aggregation kinetic parameters in 5 M urea to keep [D] fully occupied for all variants and corrected the measured $\tau_{1/2}$ at 0 M urea for each mutant with the corresponding correction factor (Table S1). These parameters transfer into the general expression for aggregation kinetics.

To correct for the general change in intrinsic aggregation propensity between $SOD1^{wt}$, $SOD1^{pwt}$, and $SOD1^{barrel}$, we determined the aggregation kinetics of the fully unfolded protein at various urea concentrations and extrapolated to 0 M urea. The offsets in $\tau_{1/2}$ between $hSOD1^{wt}$ and $SOD1^{pwt}$ and between $hSOD1^{wt}$ and $SOD1^{barrel}$ at 0 M urea are 0.34 and 0.89, respectively (Fig. S2 and Table S1).

Estimation of Protein Stability at 37 °C and Reducing Conditions. Determination of the concentrations of native (N) and unfolded (D) species at each urea concentration was by the standard two-state analysis described in refs. 14 and 59–62 and Eq. **S2**. Here, the equilibrium constant for folding is determined by the folding and unfolding rates k_f and k_u:

$$K_{D-N} = \frac{k_u}{k_f} \qquad \text{[S6]}$$

and

$$\log K_{D-N} = \log K_{D-N}^{H_2O} + m_{D-N}[\text{urea}] = \log k_u^{H_2O} + m_u[\text{urea}] - \log k_f^{H_2O} + m_f[\text{urea}], \qquad \text{[S7]}$$

where the superscript H_2O refers to the parameter value at 0 M urea and $m_{D-N} = m_u - m_f = \partial\log K_{D-N}/\partial[\text{urea}] = \partial\log k_u/\partial[\text{urea}] - \partial\log k_f/\partial[\text{urea}]$, which defines the urea dependence.

For most of the studied variants, the stability and consequently, the population unfolded have been determined at 25 °C to facilitate accurate determination of the refolding rates for highly destabilized mutants. To estimate $\log K_{DN}^{H_2O}$ at 37 °C and reducing conditions for SOD1 variants, $\log K_{D-N}^{H_2O}$ at 25 °C and 37 °C was determined for the native variants $SOD1^{wt}$, $SOD1^{pwt}$, and $SOD1^{barrel}$, and a correction term was added for variants thereof (compare with Table S2).

Exponential Aggregate Growth in Vitro and in Mice. In the in vitro aggregation assay, the monomer pool is depleted on aggregation, which results in progressive decrease of [D] during the aggregation process. Even so, in the test tube, the initial aggregation kinetics mimic the steady-state conditions in the mouse. The initial aggregation kinetics in the case where secondary pathways dominate the fibril formation have been shown to be approximately exponential with a rate constant κ (4):

$$\frac{M(t)}{c^{\text{total}}} \approx (B_+e^{\kappa t} - B_-e^{-\kappa t}) \approx \Lambda e^{\kappa t}, \qquad \text{[S8]}$$

where B_+ and B_- are proportional to κ^{-2}, and Λ is an arbitrary constant.

To obtain an estimate of the growth rate in the in vitro case with depletion of the monomer pool, we took advantage of the relationship between the lag time-τ_{lag} and the rate constant κ (4):

$$\tau_{lag} = \left[\log\left(\frac{2\kappa^2}{\lambda^2}\right) - e + 1\right]\kappa^{-1}. \quad \textbf{[S9a]}$$

Here, λ is the kinetic parameter describing formation of aggregates through primary nucleation, and κ is the kinetic parameter through secondary nucleation and/or fragmentation. These kinetic parameters are given by

$$\lambda = \sqrt{2k_+k_n[D]^{n_c}}, \quad \textbf{[S9b]}$$

where k_+ is the elongation rate, k_n is the primary nucleation rate, n_c is the primary nucleation reaction order, and

$$\kappa = \sqrt{2k_+k_-}[D]^{\gamma}. \quad \textbf{[S9c]}$$

Here, the rate is dominated by secondary nucleation, and k_- is the fragmentation rate. In the case where filament fragmentation is rate-limiting, γ equals 0.5.

We fitted the measured and corrected τ_{lag} values to Eq. **S9a**, which gave $\sqrt{2k_+k_-}$ = 1,741 h^{-1} M^{-1} and $\lambda \sim 10^{-16}$, and the concentration dependence is, as expected for a fragmentation-based aggregation, close to one-half (γ = 0.49) (Fig. 2*B*). From the experimentally determined in vitro τ_{lag}, the aggregation rate for each mutant can be determined by implicit solving of Eq. **S9a** for κ using the globally determined value $\lambda = 10^{-16}$.

The analysis of in mouse aggregation kinetic data gives the rate $\sqrt{2k_+k_-}[D]^{\gamma}$ directly. The absolute protein concentration is not known. However, the total protein concentration under overexpressing conditions has been estimated to be ∼25 μM under steady-state conditions, and of that, the population of unfolded protein has been determined to ∼3–4% for $hSOD1^{G93A}$ (37). In vitro data show that the fraction D for reduced $apoSOD1^{G93A}$ is 96%. Taken together, the cytosolic concentration of unfolded $apoSOD1^{G93A}$ can be approximated to ∼0.6 μM. For the low-expressing $hSOD1^{G93A,50\%}$ (25) mouse line and homozygous $hSOD1^{D90A}$ (25), the protein expression is 50% relative to the high $hSOD1^{G93A}$, but the population unfolded of $apoSOD1^{D90A}$ is less and estimated to be 58% (Table S3). Using these estimated concentrations of unfolded material, we can fit the rates to Eq. **S9c** and estimate $\sqrt{2k_+k_-}$ to 2.6 h^{-1} M^{-1} and γ to 0.52 (Fig. 3*D*). The concentration dependence is, thus, identical, and the mechanistic factor γ is completely independent of assumptions about absolute protein levels.

Tissue Homogenization and Epitope-Mapping Assay for SOD1 Aggregate Structure. Mice were killed by i.p. injection of pentobarbital. The spinal cords were homogenized with an Ultraturrax Apparatus (IKA) for 30 s and by sonication for 1 min in 25 volumes ice-cold PBS (137 mM NaCl, 2.7 mM KCl, 4.3 mM Na_2HPO_4, 1.4 mM KH_2PO_4, pH 7.0) supplemented with 1.8 mM EDTA, 1 mM DTT, and the antiproteolytic mixture Complete Without EDTA (Roche Diagnostics).

Quantitative staining intensity of the anti-hSOD1 peptide antibodies was as in ref. 8 and analyzed using a model free principal component analysis (PCA). The antibody binding data from nine $hSOD1^{G93A}$ terminal mice were used for PCA (Fig. 3*A*), explaining >96% of the data. In addition, data for eight samples of aggregates produced in vitro (Fig. 3*A*) were used and analyzed separately, because the principal components of the in vitro aggregates differ from the in vivo aggregates. The type B component was only present in data obtained from $hSOD1^{D90A}$ mice. The additional PCA vectors were all either at very low abundance (<0.1%) or nonphysiological, meaning that they were a mixture of positive and negative intensities.

The determined aggregate growth kinetics are independent on which antibodies are used or if the antibodies are used individually or combined in PCA to determine the kinetics (Fig. S4).

hSOD1 Turnover and Aggregation. The half-life of murine SOD1 (mSOD1) in the CNS is 20 d (63). The concentration of mSOD1 in spinal cord is 50 μg/g (wt/wt). The human SOD1 variants in most transgenic models are expressed at about 25-fold greater rates (25). The G93A mice are exceptional and express SOD1 at rates 40-fold higher. In terminal ALS model mice, the concentrations of aggregated SOD1 in spinal cord are about 70 μg/g (wt/wt) (8). Under steady-state conditions, the daily turnover of mSOD1 is, thus, ln2 × 1/20 × 50 = 1.73 μg/g. In the transgenic models, it should be 25 × 1.73 = 43.3 μg/(g·d). [G93A = 69 μg/(g·d)]. Thus, the total amount of aggregates corresponds to 1.63 d of synthesis in the whole tissue.

Motor neurons are estimated to account for 20% of the volume of ventral horns (64). The ventral horns, in turn, account for about 20% of the area of the spinal cord. Thus, crudely, the motor neurons can be estimated to occupy 4% of the spinal cord volume. Furthermore, assuming homogeneous synthesis rates throughout the spinal cord, the motor neurons in G93A mice are expected to synthesize SOD1 at 0.04 × 69 = 2.8 μg/(g·d). Using the 16-d doubling time determined for the G93A mice, the rate of aggregation in the terminal stage can be calculated to 70 × ln2/16 = 3.0 μg/(g·d). The situation is, of course, complex with loss of motor neurons, but also, there is likely involvement of other cell types in SOD1 aggregation. Still, even allowing for uncertainties in some of the assumptions made, it would appear that, when the terminal stage is reached, virtually all SOD1 that is synthesized becomes recruited into aggregates.

SOD1 Aggregation Mechanism Is Independent on Small Differences in pH. To assure that small differences in pH between the in vitro experiments (pH 6.3) and the in vivo experiments do not change the aggregation mechanism, we determined the pH dependence of the fibrillation kinetics using urea to tune protein stability as described in ref. 7. The results show that the impact of His protonation in the pH 6.3–7.4 range is negligible and overlaps with data from mutational destabilization (Fig. S3). As shown in Fig. S3, the protein stability and fibrillation kinetics at pH 6.3 and pH 7.4 are indistinguishable, with deviations appearing first on titration of the carboxylate groups below pH 5.5. Even under these acidic conditions, however, the effect of pH is simply coupled to the pH-induced decrease of monomer stability, which is accounted for in log[D] on the *x* axis. The $\log\tau_{1/2}$ dependence on log[D] remains the same with $\gamma^{\text{in vitro}}$ = 0.4–0.5, and there is by no measure any change of the aggregation mechanism.

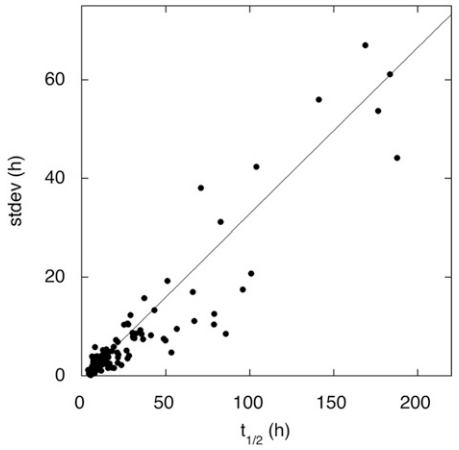

Fig. S1. The approximately linear correlation between the measured $\tau_{1/2}$ and the experimental SD [SD($\tau_{1/2}$)] indicates that the aggregation of hSOD1 is a stochastic event.

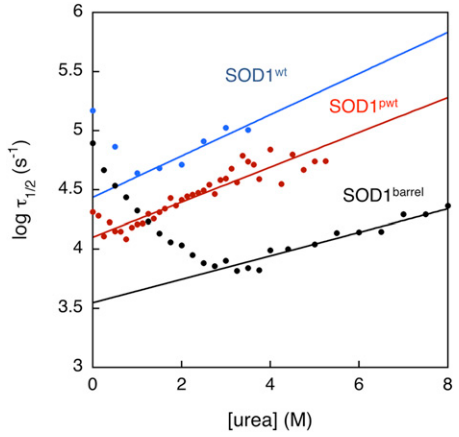

Fig. S2. Fibrillation data. Fibrillation half-times ($\tau_{1/2}$) for $hSOD1^{wt}$, $SOD1^{pwt}$, and $SOD1^{barrel}$ vs. [urea] derived from the fibrillation time courses described in ref. 7. The offsets in $\tau_{1/2}$ between $hSOD1^{wt}$ and $SOD1^{pwt}$ and between $hSOD1^{wt}$ and $SOD1^{barrel}$ at 0 M urea are 0.34 and 0.89, respectively.

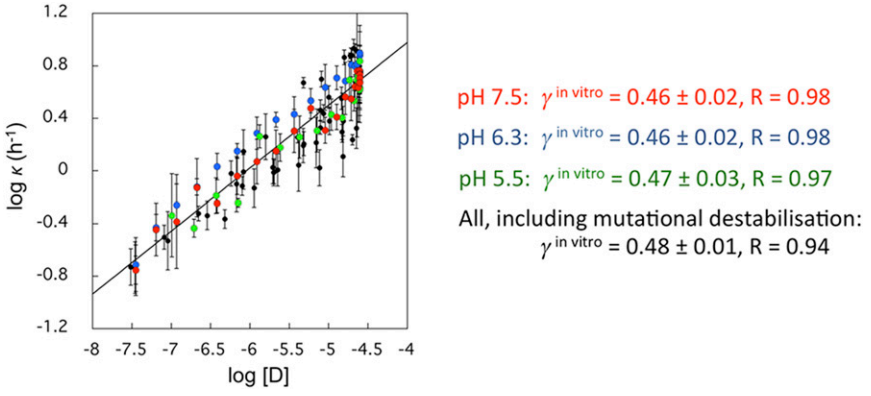

Fig. S3. Plot of logκ as a function of log[D] showing that the aggregation mechanism is independent on changing the pH from 5.5 (green) to 6.3 (blue) and further, to 7.5 (red). Here, [D] is varied over three orders of magnitude using urea to modulate SOD1 stability. The black markers correspond to aggregation kinetics, where mutations are used to modulate [D].

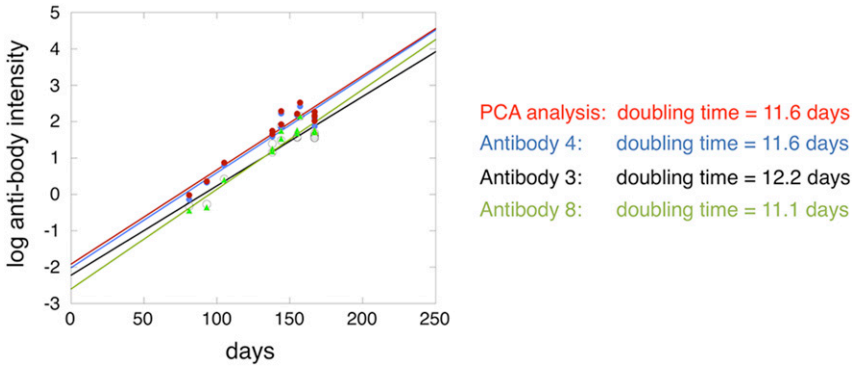

Fig. S4. Control of aggregate growth kinetics in hSOD1^{G93A} mice using three different antibodies (amino acids 43–57, 57–72, and 131–153) individually as well as combined using PCA. The determined doubling times $\tau_{x2} = \ln 2/\kappa$ is the same independent of the antibody used.

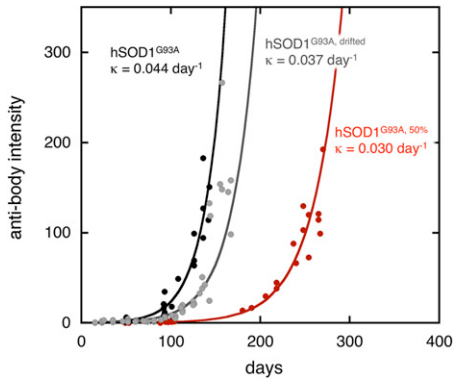

Fig. S5. Exponential aggregate growth in three lines of transgenic mice expressing the ALS-associated SOD1 mutation G93A at different expression levels. Black and red traces are from Fig. 3, and gray shows hSOD1^{G93A} mice with 12% copy number loss (8). Kinetic data are in Table S3.

Table S1. Parameters for fibrillation kinetics and protein stability in vitro

SOD1 variant	$\log \tau_{1/2}$(h)*	$\log \nu_{max}$(h^{-1})*	p^{mut}/p^{wt} ‡	$\log \tau_{1/2}$(h)§	logκ(h^{-1})¶	$\log K_{D-N}^{H_2O}$ 25°C ox#	$\log K_{D-N}^{H_2O}$ 37°C red‖	$\log fc^{total}$(M)**
$hSOD1^{wt}$	1.61	−0.60	0.00	1.61	−0.12	−3.30	−1.48	−6.10
L84V	1.14	−0.18	−0.05	1.20	0.38	−0.85	−0.16	−4.99
D90A	1.28	0.07	−0.17	1.45	−0.01	−1.74	−1.05	−5.69
G93A	0.79	−0.17	−0.08	0.87	0.87	−0.44	0.25	−4.80
I113T	0.87	0.33	0.01	0.88	0.67	−1.31	−0.62	−5.32
$SOD1^{pwt}$	0.76	0.10	0.00	1.10	0.44	−2.17	−0.28	−5.07
A4V	0.69	0.25	−0.04	1.06	0.67	−1.04	0.85	−4.66
L84V	0.65	0.17	0.35	0.64	0.91	−0.85	1.04	−4.64
G85R	0.50	0.37	−0.03	0.87	0.74	−0.81	1.08	−4.64
D90A	0.54	0.39	−0.07	0.95	0.55	−1.74	0.15	−4.84
G93A	0.55	0.28	0.04	0.85	0.71	−0.44	1.45	−4.62
I99A	0.64	0.28	0.29	0.70	0.88	−1.40	0.48	−4.73
I112A	0.54	0.66	0.30	0.58	0.93	−1.19	0.70	−4.68
I113T	0.63	0.11	0.29	0.68	0.88	−1.31	0.58	−4.70
L144A	0.64	0.17	0.06	0.92	0.56	−2.20	−0.32	−5.09
L144F	0.65	0.30	0.01	0.98	0.56	−2.06	−0.17	−5.00
C6/57/111/146A	0.71	0.02	−0.03	1.08	0.46	−1.16	−0.34	−5.10
$SOD1^{barrel}$	1.34	−0.38	0.00	2.23	−0.75	−3.75	−2.85	−7.45
L8A	0.59	0.33	0.20	1.28	0.30	−0.73	0.16	−4.83
V14A	1.04	−0.06	0.03	1.90	0.34	−2.83	−1.94	−6.54
I18A	0.63	0.38	0.32	1.19	0.33	−1.24	−0.34	−5.11
F20A	0.52	0.44	0.29	1.12	0.32	0.07	0.96	−4.65
V29A	0.50	0.52	0.13	1.26	0.26	−1.61	−0.72	−5.39
V31A	0.80	0.16	0.14	1.55	−0.02	−2.52	−1.63	−6.24
I35A	0.62	0.38	0.40	1.11	0.38	−0.69	0.20	−4.81
L38A	0.67	0.43	0.08	1.48	0.02	−1.25	−0.35	−5.12
F45A	0.70	0.30	0.26	1.33	0.21	−1.52	−0.62	−5.32
V47A	0.81	0.14	0.19	1.51	−0.01	−1.96	−1.06	−5.70
L84A	0.74	0.35	0.15	1.49	0.01	−1.90	−1.01	−5.65
V87A	0.85	0.09	0.11	1.64	−0.10	−2.45	−1.55	−6.17
V97A	0.94	0.06	0.39	1.44	0.19	−1.53	−0.63	−5.32
I99A	1.07	−0.01	0.14	1.83	−0.36	−2.61	−1.71	−6.32
V103A	1.46	−0.51	0.09	2.26	−0.75	−3.75	−2.86	−7.46
I104A	0.66	0.19	0.22	1.33	0.26	−2.07	−1.17	−5.80
L106A	0.75†	0.05†	0.27	1.37	0.24	−0.28	0.62	−4.70
I112A	0.84	0.00	0.19	1.54	−0.01	−2.36	−1.47	−6.08
I113A	0.79	0.08	0.18	1.50	0.03	−1.97	−1.07	−5.71
L117A	0.63	0.20	0.09	1.44	0.15	−2.36	−1.47	−6.08
V119A	0.51	0.42	0.12	1.28	0.21	−1.31	−0.41	−5.16
L144A	1.31	−0.36	0.20	2.00	−0.50	−3.38	−2.49	−7.09
I149A	0.69	0.13	0.15	1.43	0.11	−0.70	0.20	−4.82
I151A	1.11	−0.09	−0.01	2.02	−0.53	−3.34	−2.44	−7.04
H43A	0.89	−0.11	0.07	1.71	−0.13	−2.22	−1.33	−5.95
H43F	1.43	−0.40	0.05	2.27	−0.73	−3.81	−2.91	−7.51
L117V	1.03	−0.14	0.03	1.90	0.32	−2.94	−2.05	−6.65
G93A	0.60	0.84	0.03	1.46	0.04	−1.60	−0.70	−5.38

Data refer to reducing conditions at pH 6.3 and 37 °C unless otherwise stated.

*Averages of 6–198 experiments.

†Average of 3 experiments.

‡Measured from $\tau_{1/2}^{mutant}/\tau_{1/2}^{wt}$ under standard conditions when the protein is fully unfolded.

§Corrected for p^{mutant}/p^{wt} and offset between $hSOD1^{wt}$, $SOD1^{barrel}$, and $SOD1^{pwt}$.

¶Calculated from Eq. **3**.

#$\log K_{D-N} = \log K_{D-N}^{H_2O} + m_{D-N}[\text{urea}] = \log k_u^{H_2O} + m_u[\text{urea}] - \log k_f^{H_2O} + m_f[\text{urea}]$.

‖Measured directly at 37 °C or calculated from folding kinetics under oxidizing conditions at 37 °C according to Table S2.

Calculated from Eq. **2.

Table S2. Protein stability and correction term for estimation of $\log K_{D-N}^{H_2O}$ at 37 °C and reducing conditions

	$\log K_{D-N}^{H_2O}$ 25 °C ox	$\log K_{D-N}^{H_2O}$ 25 °C red	$\log K_{D-N}^{H_2O}$ 37 °C ox	$\log K_{D-N}^{H_2O}$ 37 °C red	Correction
$SOD1^{pwt}$	−2.17	−0.95	−1.79	−0.28	1.87*
$hSOD1^{wt}$		−2.15		−1.48†	0.67‡
$hSOD1^{mutants}$					1.20§
$SOD1^{barrel}$	−3.75	—	−2.85	—	0.90¶

*Calculated from the differences in $\log K_{D-N}^{H_2O}$ between oxidized and reduced $SOD1^{pwt}$ at 25 °C and 37 °C. This value was used to estimate $\log K_{D-N}^{H_2O}$ at 37 °C for mutant $SOD1^{pwt}$ (Table S1).
†Estimated by adding the differences in $\log K_{D-N}^{H_2O}$ between reduced $SOD1^{pwt}$ at 25 °C and 37 °C to $\log K_{D-N}^{H_2O}$ of reduced $hSOD1^{wt}$ at 25 °C.
‡Calculated from the differences in $\log K_{D-N}^{H_2O}$ between reduced $SOD1^{pwt}$ at 25 °C and 37 °C.
§Calculated from the differences in $\log K_{D-N}^{H_2O}$ between reduced $SOD1^{pwt}$ and reduced $hSOD1^{wt}$ at 37 °C. This value was used to estimate $\log K_{D-N}^{H_2O}$ at 37 °C for mutant hSOD1 (Table S1).
¶Calculated from the differences in $\log K_{D-N}^{H_2O}$ between $SOD1^{barrel}$ at 25 °C and 37 °C. This value was used to estimate $\log K_{D-N}^{H_2O}$ at 37 °C for mutant $SOD1^{barrel}$ (Table S1).

Table S3. Survival, fibrillation kinetics, and protein concentration in vivo

	Survival time (d)*	mRNA†	f	$[D]/c^{total}$‡	logκ§ (d^{-1})
$hSOD1^{wt}$	367	80¶	0.34	0.25	
$hSOD1^{G85R}$	345	43	0.92	0.40	
$hSOD1^{D90A}$	407	51	0.58	0.30	−1.61
$hSOD1^{G93A}$	124	100	0.96	0.96	−1.36
$hSOD1^{G93A,50\%}$	253	50	0.96	0.48	−1.51
$hSOD1^{G93A,drifted}$	155	88¶	0.96	0.85	−1.43
$hSOD1^{127X}$	203	63	1	0.63	
$hSOD1^{127X,50\%}$	416	32	1	0.32	

*Average time to reach terminal stage.
†Determined as described in ref. 25.
‡Calculated from $[D]/c^{total} = fX/X^{ref}$.
§Calculated from single exponential fit to data in Fig. 3*B*.
¶Corrected for 12% copy number loss.